Numerical and Analytical Investigation on the Influence of Geometry on Thermohydraulic Performance of Single-phase Split Flow Cold Plates for Data Center Liquid Cooling

*Deogratius Kisitu, Alfonso Ortega

NSF – Center for Energy-Smart Electronic Systems (ES2), Villanova University, Villanova, PA, USA *dkisitu@villanova.edu

Abstract—Split flow impingement microchannel cold plates are being actively deployed in liquid cooling for high heat density data center thermal management. In contrast to the conventional parallel flow scheme, split flow configuration cold plates have a central slot/slit that divides the flow into two branches thus halving the flow rates and flow lengths, which in return reduces the pressure drop and increases the heat transfer coefficient as a result of the influence of the thermally developing flow for shorter flow lengths. In this paper, laminar flow CFD and a new approximate analytical model were utilized to investigate the performance of split flow microchannel cold plates. The effects of jet-slot aspect ratio (ratio of jet-slot width to cold plate channel length), β, channel aspect ratio, α , and fin tilt angle, θ , were investigated in detail. The performance of a split flow cold plate and a counterpart geometrically identical parallel flow cold plate was also compared under the same conditions. Results show that increasing the jet slot aspect ratio reduces pressure drop with a slight increase in the thermal resistance. The thermal resistance weakly depends on fin tilt angle, but pressure drop monotonically increase with decreasing fin tilt angle. It is shown that an optimum channel aspect ratio of about $\alpha=12$ minimizes thermal resistance, whereas increasing channel aspect ratio decreased the pressure drop. Results reveal that geometrically identical split flow and parallel flow cold plates have similar thermal resistance, but the split-flow configuration exhibits significantly lower pressure drop.

Keywords—Liquid cooling, Split flow, Microchannel cold plates, Impingement, CFD, Analytical models, Electronic cooling, Data centers

NOMENCLATURE

Α	Area, m ²
b	Channel width, m
c_p	Specific heat, J/kgK
$\dot{D_h}$	Channel hydraulic diameter, m
f	Fanning friction factor
$rac{f}{h}$	Average heat transfer coefficient, W/m ² K
Н	Height, m
k	Thermal conductivity, W/mK
K_c	Contraction coefficient
K_e	Expansion coefficient

L	Base plate length, m
l_{eff_1}	Effective length of the vertical channel, m
l_{eff_2}	Effective length of the horizontal channel, m
$L_{ m eff}$	Proposed total effective flow length, m
L_h	Hydrodynamic entrance length, m
L_{th}	Thermal entrance length, m
ṁ	Mass flow rate, kg/s
N	Number of channels
NTU	Number of transfer units
\overline{Nu}	Average Nusselt number
Pr	Prandtl number
P	Pressure, Pa
ġ	Total heat transfer rate, W
$q^{\prime\prime}$	Heat flux, W/cm^2
Re	Reynolds number
R	Thermal resistance, K/W
t	Fin thickness, m
T	Temperature, K
U	Average velocity, <i>m/s</i>
W	Width, m
x^+	Dimensionless hydrodynamic channel length
x^*	Dimensionless thermal channel length

Greek Symbols

β	Jet slot aspect ratio
3	Effectiveness of a cold plate
σ	Fin array porosity
θ	Tilt angle, °
ho	Density, kg/m ³
η_{fin}	Fin efficiency
η_o	Overall surface efficiency
ΔΡ	Pressure drop, Pa
ν	Kinematic viscosity, m ² /s
μ	Dynamic viscosity, Pa s

Channel aspect ratio

Subscripts

avg Area-averaged

base Base chan Channel Conductive condCopeland cop Chip С cpCold plate eff Effective fin fd Fully-developed Hydrodynamically-developing hdliq Liquid Bulk mean m i Inlet 0 Outlet S SISE Solid Spreading sp Total tot T TISE Wall w

I. INTRODUCTION

The advance in modern, high-performance electronics is causing rapid increase in the heat fluxes that need to be cooled to maintain allowable junction temperatures [1], [2], [3]. Currently, air-cooling is approaching its limits in many high heat density electronics [2] thereby increasing the need for high performance indirect liquid cooling using cold plates [1], [4]. Parallel flow microchannel cold plates are among the most common configurations currently in use due to their relatively high performance and manufacturability [5].

Kandlikar [6], and Kisitu and Ortega [3] previously reported that parallel flow or single-pass or side-in side-exit (SISE) flow of liquid coolant through the microchannel cold plate is not optimal due the associated higher pressure drop derived from longer flow lengths and required higher mass flow rates to meet the thermal goal. Split flow or top-in side-exit (TISE) microchannels are an alternative configuration that has been previously utilized in both air and liquid cooled heat sinks and cold plates [2], [3], [6], [7]. Split flow cold plates have a central inlet slot that divides the incoming flow into two branches thereby halving the flow rate and flow path/length, which reduces the pressure drop. Although the heat transfer coefficient may be enhanced due to the developing flow in the shortened flow length, the flow rate is reduced by 50% and therefore it is not immediately obvious whether or not the split flow leads to increased thermal performance.

In contrast to the traditional parallel flow liquid-cooled cold plates which can be readily modelled when the flow is laminar [5], the more complex flow path in the vicinity of the impingement zone prevents does not allow for an analytical solution for the flow or temperature field. Most of the previous split flow cold plate studies are numerical and experimental. Sung and Mudawar [8] studied single-phase liquid cooling performance of a split flow microchannel module using HFE-7100 as a working fluid. They conducted 3-D CFD simulations

to both study single-phase flow performance and obtain the optimal geometry for the maximization of heat rejection and temperature uniformity while minimizing the average surface temperature. Experiments followed for the validation of the CFD findings, which were also handy in developing correlations for heat transfer coefficients for the split flow microchannels. In another study, Hadad et al. [9] conducted CFD modeling of a warm water-cooled split flow microchannel cold-plate, with a V-grooved slot. Their goal was to predict thermohydraulic performance and optimize the split flow microchannel geometry. In a similar investigation, Hadad et al. [10] developed a numerical model for a V-grooved slot split flow microchannel cold plate and studied effects of inlet and outlet manifolds (distributor and collector) on cold plate thermohydraulic performance. Their CFD model was utilized in shape optimization of the split flow cold plate. In other related work, Ramakrishnan et al. [11] experimentally investigated a commercial warm water-cooled split flow microchannel cold plate. They reported experimental data for thermal resistance and pressure drop of this split flow cold plate and used a resistance network model to compute the effective heat transfer coefficient.

Kisitu and Ortega [3] recently developed a new physics-based analytical model based on an equivalent parallel flow concept, where a total effective flow length, $L_{\rm eff}$ of a split flow microchannel was expressed as the sum of the two effective flow lengths $l_{\rm eff_1}$ and $l_{\rm eff_2}$. The effective flow lengths were obtained from Duan and Muchyka's model for air-cooled split flow macrochannel heat sinks [12]. Over a wide range of geometric and flow parameters, the thermal resistance and pressure drop predictions from the proposed split flow microchannel cold plate analytical models [2], [3] agreed well with the 3D laminar CFD simulations.

In this present study, 3D laminar flow CFD and the previously proposed new approximate analytical model [2], [3] were used to examine influence of split flow geometric variables, including jet-slot aspect ratio, β , channel aspect ratio, α , and fin tilt angle, θ , on the split flow performance. Additionally, the thermohydraulic performance of a split flow cold plate and a geometrically identical parallel flow cold plate were compared under the same thermal and flow conditions.

I. CFD AND ANALYTICAL MODELING

In this section, the numerical or CFD models for split flow and parallel flow microchannel cold plates are detailed. In addition, the analytical physics-based thermohydraulic models for split flow microchannels, which were developed and validated in [2], [3] and dubbed the 'equivalent parallel flow models', will be summarized and used in the present parametric analysis.

- A. CFD Modeling (Simulations)
- 1) Modeling Assumptions

In the current numerical/CFD modeling, the following assumptions were taken.

• Isoflux or constant heat flux at the cold plate base

- 3-D and laminar flow
- Constant thermophysical properties of water and copper
- Gravity and other body forces effected are neglected
- Split flow microchannels are all both thermally and hydraulically identical and hence a single symmetric or half split flow microchannel is taken as a computational domain because of symmetry
- Steady state flow and incompressible fluid

2) Governing Equations

The governing equations (Navier Stokes and energy equations) for this conjugate heat transfer problem are:

• Conservation of mass or continuity for liquid

$$\nabla \cdot \vec{V} = 0 \tag{1}$$

• Momentum equation for liquid

$$\rho_{liq}(\vec{V}.\nabla)\vec{V} = -\overline{\nabla}\vec{P} + \mu_{liq}\nabla^2\vec{V}$$
 (2)

• Energy equation for liquid

$$\rho_{liq}c_{p,liq}(\vec{V}.\nabla)T_{liq} = k_{liq}\nabla^2 T_{liq}$$
 (3)

Energy equation for solid

$$\nabla^2 T_s = 0 \tag{4}$$

3) CFD Domain and Boundary Conditions

For the vertical-finned split flow cold plate microchannels, the computational domain is modeled as a half of a unit cell of the split flow microchannel due to symmetry [3], as shown in Fig. 1, with all boundary conditions detailed. The domain for the tilted-finned split flow cold plate microchannels, as shown in Fig. 2, is similar to that vertical-finned case, except that a periodic boundary condition is introduced on the symmetric sides in the tilted-finned case [2], [3].

On the other hand, due to symmetry, a single unit cell of the microchannel array was considered as the numerical domain for the parallel flow cold plate microchannel [2], as illustrated in Fig. 3, with delineated boundary conditions.

For both split flow and parallel flow domains, a constant pressure drop boundary condition is applied at the exit of microchannel unit cells. An isoflux (constant heat flux) condition was applied to the bases of both unit cell microchannels to simulate the heat generation from the chip.

4) CFD (Numerical) Method

Computational fluid dynamics (CFD) modeling was attained by conducting ANSYS/Fluent 3-D simulations. Patankar's finite volume method called Semi-Implicit Method for Pressure Linked Equations (SIMPLE) algorithm, was used to numerically solve the Navier-Stokes equations. A second-order upwind scheme was utilized to discretize the Navier-Stokes equations and energy equation.

Grid sensitivity or independence analyses were conducted based on thermal resistance and pressure drop (area-averaged

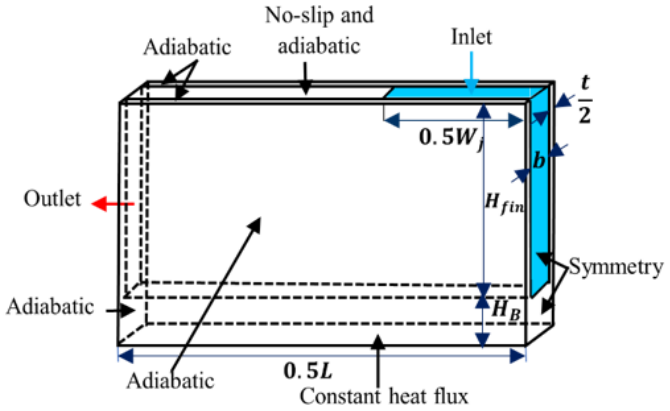


Fig. 1. Computational domain for a vertical finned ($\theta = 90^{\circ}$) split flow symmetric/half unit cell microchannel

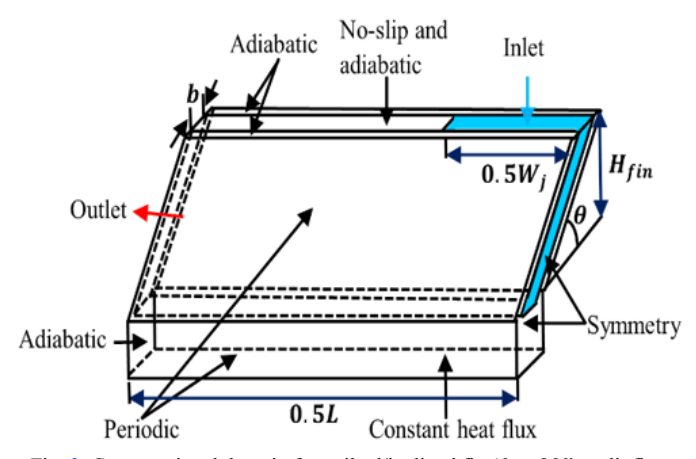


Fig. 2. Computational domain for a tilted/inclined fin ($\theta < 90^{\circ}$) split flow symmetric/half unit cell microchannel

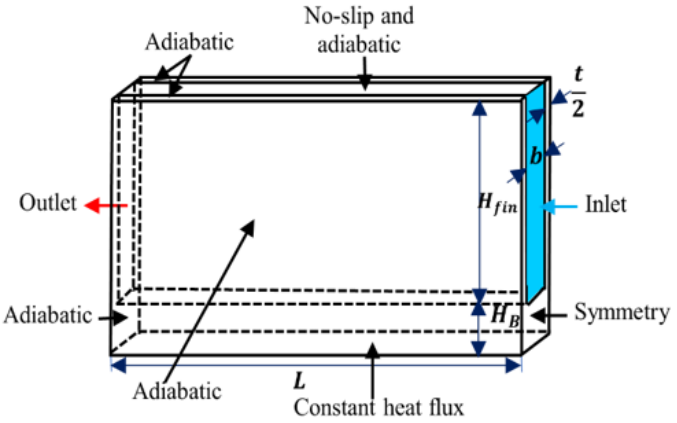


Fig. 3. Computational domain for a parallel flow unit cell microchannel

pressures differences between the inlet and the outlet of the symmetric unit cell microchannel), as defined in Eqns. 5 and 6. Grid independence analyses were performed, for both split flow (Fig. 4) and parallel flow (Fig. 5) unit cell microchannels, by varying the number of cells from 20,000 to 492,800 and 20,000 to 500,000, respectively. A grid with 300,000 cells was suitably considered for both split flow and parallel flow unit cells for the present numerical modeling.

$$R_{th} = \frac{\left(T_{base} - T_{m_i}\right)}{q_R''} \tag{5}$$

$$\Delta P = P_{avg,i} - P_{avg,o} \tag{6}$$

It should be noted that the same CFD model used in [2], [3] is being used in this parametric study. The CFD model was already validated against experimental data and analytical models in [2], [3], with good accuracy/agreement reported. As such, there is confidence in accuracy of the CFD simulations results for the present investigations.

5) CFD Simulations for Parametric Analysis

Initially, CFD simulations of split flow microchannel are performed while varying vital geometric parameters including the jet slot aspect ratio, β , channel aspect ratio, α , and fin tilt angle, θ .

Fig. 6 and 7 show the ANSYS velocity vector plot (liquid phase) and isothermal contour plots (solid and liquid phase), respectively, for the split flow cold plate half unit cell microchannel. The existence of flow separation and stagnation zones due to turning flow in split flow configuration are illustrated in Fig. 6.

Lastly, numerical simulation were conducted on parallel flow cold plate, geometrically identical to split flow counterpart, and results compared to investigate the effect of flow configuration on thermohydraulic performance of the microchannel cold plates. For all simulations conducted, both split flow and parallel flow cold plates have 100 microchannels, with general geometric dimensions shared by these two kinds of cold plates, as shown in Table. 1.

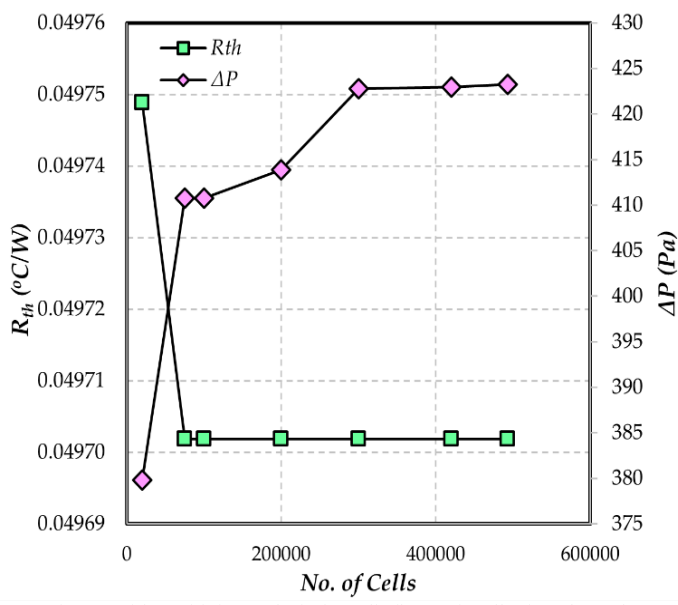


Fig. 4. Grid sensitivity analysis for split flow unit cell microchannel

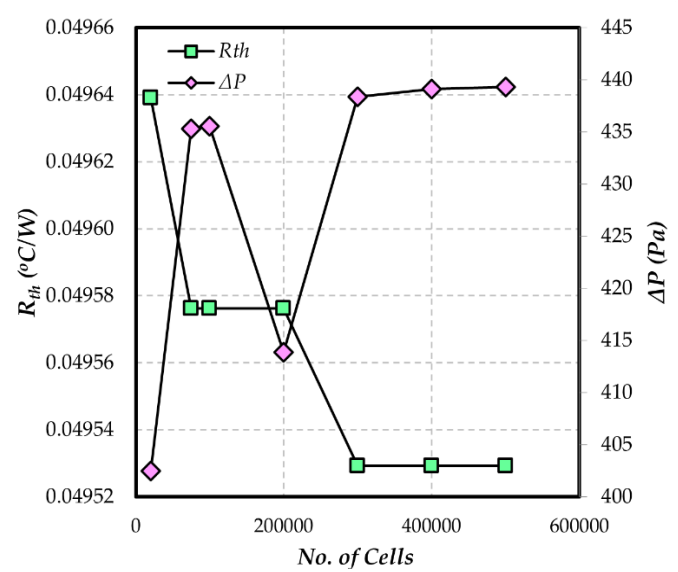


Fig. 5. Grid sensitivity analysis for parallel flow unit cell microchannel

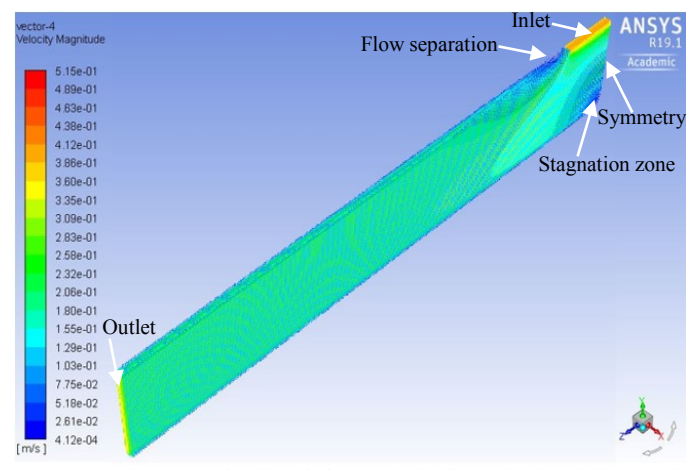


Fig. 6. Velocity vector plot (liquid phase) of split flow cold plate half unit cell microchannel with $\beta = 0.1$ and $T_{in} = 300$ K

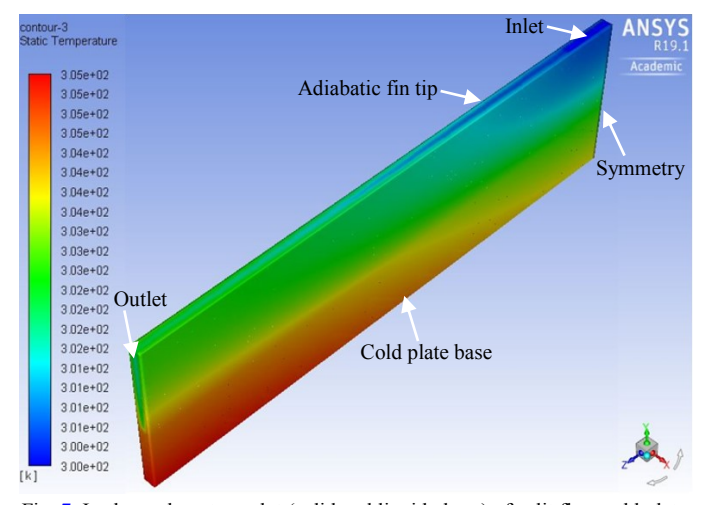


Fig. 7. Isothermal contour plot (solid and liquid phase) of split flow cold plate half unit cell microchannel with $\beta = 0.1$ and $T_{\rm in} = 300 K$

Additionally, thermal boundary condition was identical for all simulated cases, where substrate metal was copper and a constant heat flux of $q_B'' = 27W/cm^2$ was applied at the bases of the cold plate unit cell microchannels. In the same sense, the flow conditions were all the same, with pure water as the working fluid and the inlet fluid temperature of 27 °C. Thermophysical properties of water and copper were considered constant at 27 °C, as shown in Table. 2.

TABLE 1. GEOMETRIC DIMENSIONS SHARED BY SPLIT FLOW AND PARALLEL FLOW SIMULATED COLD PLATES [3]

L(mm)	W (mm)	b (µm)	$H_b(mm)$	t (mm)	N_{ch}
23.6	27	167	1.35	0.1	100

TABLE 2. TPROPERTIES OF WATER AND COPPER AT 27 °C [3]

Material	$\rho (kg/m^3)$	$\mu (kg/m.s)$	$c_p\left(J/kg.K\right)$	k(W/m.K)
Water	997	0.000855	4179	0.613
Copper	8978		381	388

B. Analytical (Approximate) Model

1) Split Flow Microchannel Cold Plate Analytical Modeling

Thermohydraulic laminar analytical models for split flow cold plates developed and validated in [2], [3] based on an equivalent parallel flow concept were used in the present geometrical parametric analyses of the split flow microchannel cold plate. The effective flow length l_{eff} , shown in Fig. 8, in the equivalent parallel flow model for split flow liquid-cooled microchannel cold plate [3] to be used in the present analytical modeling, was determined from the similar model by Duan and Muzychka [12] for air cooled macrochannel split flow heat sink, shown in Fig. 9.

a) Thermal Analytical Model

i. Heat Transfer Coefficient, \bar{h} Model

The split flow microchannels' average heat transfer coefficient, \overline{h} , basing on the bulk mean fluid temperature, is defined as [3]:

$$\bar{h} = \frac{1}{L_{eff}} \int_{0}^{L_{eff}} h(x) dx = \frac{1}{L_{eff}} \int_{0}^{L_{eff}} \left(\frac{q_x''}{[T_W - T_b(x)]} \right) dx \quad (7)$$

 \overline{h} can also be defined as a function of Nusselt number \overline{Nu} , thermal conductivity and hydraulic diameter.

$$\bar{h} = \overline{Nu} \left(\frac{k_{liq}}{D_h} \right) \tag{8}$$

Using a correlation by Copeland [13], for both fully developed and developing laminar flow, \overline{Nu} is predicted based on bulk mean fluid temperature

$$\overline{Nu} = \left\{ \left[2.22 \left(x_{eff}^* \right)^{-0.33} \right]^3 + (\overline{Nu}_{fd,cop})^3 \right\}^{1/3} \tag{9}$$

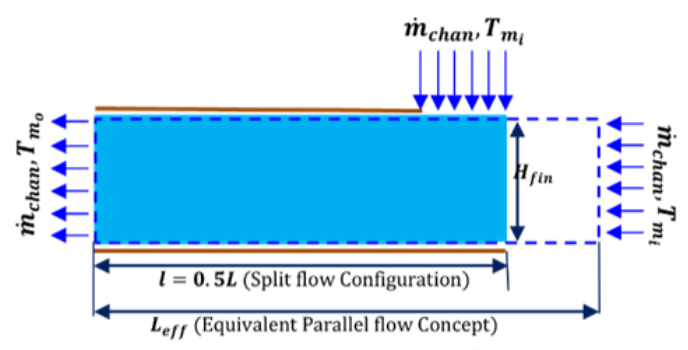


Fig. 8. Kisitu and Ortega model (equivalent parallel flow concept model) for split flow liquid-cooled microchannel cold plate [3]

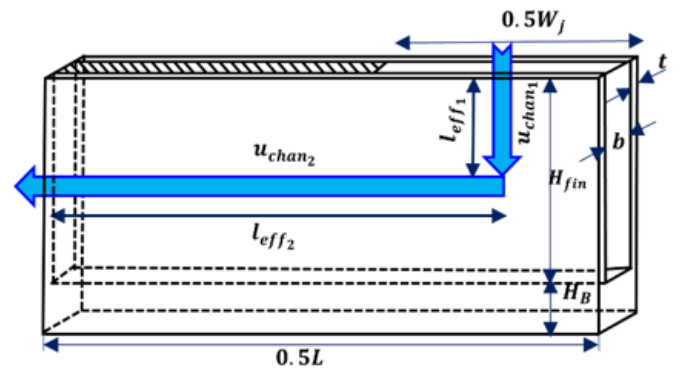


Fig. 9. Duan and Muchyka model for split flow air-cooled macrochannel heat sink [3], [12]

Where,

The fully developed flow Nusselt number model, $\overline{Nu}_{fd,cop}$ is defined as

$$\overline{Nu}_{fd,cop} = 8.31G - 0.02 \tag{10}$$

$$G = \frac{[(1/\alpha)^2 + 1]}{[1/\alpha + 1]^2} \tag{11}$$

$$\alpha = \frac{H_{fin}}{h} \tag{12}$$

And hydraulic diameter is defined as a function channel spacing, b, channel aspect ratio, α , and fin tilt angle, θ [3]:

$$D_h = \frac{2b \sin \theta}{\left(1 + \frac{1}{\alpha} \sin \theta\right)} \quad \text{for } 0^{\circ} < \theta \le 90^{\circ}$$
 (13)

For high α and vertical fins, D_h reduces to Eqn. 14 as expected:

$$D_h = 2b$$
 for $\theta = 90^{\circ}$, $\alpha >> 1$ (14)

The channel Reynolds number is defined as below [3]:

$$Re_{D_h} = \left(\frac{U_j D_h}{v_{lig}}\right) \left(\frac{W_j}{H_{fin}}\right) \tag{15}$$

The dimensionless thermal length is defined [3]:

$$\chi_{eff}^* = \frac{(L_{eff}/D_h)}{Re_{D_h}Pr} \tag{16}$$

The equivalent parallel flow length, L_{eff} for a split flow symmetric microchannel unit cell is defined as [3]:

$$L_{\rm eff} = l_{\rm eff_1} + l_{\rm eff_2} \tag{17}$$

Where.

$$l_{\rm eff_1} = 0.5 H_{fin} \tag{18}$$

$$l_{\text{eff}_2} = 0.5L - 0.25W_i \tag{19}$$

 L_{eff} can also be defined as a function of L, β and H_{fin} [3]:

$$L_{\text{eff}} = 0.5[(1 - 0.5\beta)L + H_{fin}] \tag{20}$$

Where the jet slot aspect ratio, β (ratio of jet slot width to channel length) is expressed as:

$$\beta = \frac{W_j}{I} \tag{21}$$

ii. Thermal Resistance Model

The overall thermal resistance model of the split flow cold plate was derived [2], which is a function of heat exchanger effectiveness (ε_T) , and similar to a model developed by Copeland [13]

$$R_{cp} = \frac{1}{\dot{m}_{cp}c_p\varepsilon_T} = \frac{1}{\dot{m}_{cp}c_p(1 - e^{-NTU_T})}$$
 (22)

Where,

$$NTU_T = \frac{\eta_{o,T} A_{w,T} \bar{h}}{\dot{m}_{cp} c_p} \tag{21}$$

$$A_{w,T} = N_{fin}.(2H_{fin}.(L_T + t)) + N_T.b.L_T$$
 (22)

$$L_T = 2L_{\rm eff} \tag{23}$$

$$\eta_o = 1 - \frac{2A_f}{A_{w,T}} (1 - \eta_{fin})$$
(24)

$$\dot{m}_{cp} = N_{S}.\dot{m}_{chan} \tag{25}$$

The base plate conductive thermal resistance of the split flow cold plate is be given by [3].

$$R_{cond} = \frac{H_B}{k_B A_B} \tag{26}$$

where,

$$A_R = W_R.L \tag{27}$$

The spreading thermal resistance in the cold plate base is computed from a model by Lee [14], as defined in Eqn. 27.

$$R_{sp} = \frac{\left(\sqrt{A_B} - \sqrt{A_C}\right)}{k_B \sqrt{\pi A_B A_C}} \frac{\left(\lambda k_B A_B R_{cp} + \tanh(\lambda H_B)\right)}{\left(1 + \lambda k_B A_B R_{cp} \tanh(\lambda H_B)\right)} \tag{28}$$

where.

$$\lambda = \frac{\pi^{1.5}}{\sqrt{A_R}} + \frac{1}{\sqrt{A_C}} \tag{29}$$

The total thermal resistance for the split flow microchannel cold plate is then modeled by adding up all the pertinent thermal resistances [3].

$$R_{th} = R_{cp} + R_{cond} + R_{sp} \tag{30}$$

b) Hydraulic Model

The equivalent parallel concept model [3] is also used in the present analytical hydraulic modeling of split flow microchannel cold plates. The pressure drop of a split flow split flow microchannel is a function of the total effective length, $L_{\rm eff}$ as defined in [3].

$$\Delta P_{cp} = \frac{\rho_{liq} u_{chan}^2}{2} \left[\frac{4f L_{eff}}{D_h} + (K_c + K_e) \right]$$
 (31)

The expansion (K_e) and contraction (K_c) loss coefficients are defined as functions of fin array porosity (σ) [15].

$$\sigma = \frac{b}{b+t} \tag{32}$$

$$K_c = 0.8 - 0.4\sigma^2 \tag{33}$$

$$K_e = 1.0(1 - \sigma)^2 - 0.4\sigma \tag{34}$$

Using a model by Copeland [13], the Fanning friction factor, f for fully developed laminar flow in the equivalent parallel flow channels of split flow cold plate microchannels is defined as an function of channel aspect ratio.

$$f = \frac{(19.64G + 4.7)}{Re_{Dh}} \tag{35}$$

For hydrodynamically developing and laminar flow, the apparent friction factor is defined as a function of dimensionless hydraulic effective flow length, x^+_{eff} [3];

$$f_{hd} = \frac{\left[\left(3.2 \left(x_{eff}^+ \right)^{-0.57} \right)^2 + (f R e_{Dh})^2 \right]^{0.5}}{R e_{Dh}}$$
 (36)

Where.

$$x^{+}_{eff} = \left(\frac{L_{\text{eff}}}{D_{h}}\right) / Re_{D_{h}} \tag{37}$$

 Parallel Flow Microchannel Cold Plate Analytical Modeling

a) Thermal Analytical Model

The Nusselt number to compute the heat transfer coefficient in the parallel flow microchannels is modeled using Copeland's model [13] as described for the split flow case, except that the flow length changes from $L_{\rm eff}$ to L for parallel flow.

The cold plate thermal resistance is obtained from a model by Zhang, et al. [5], which was validated experimentally in [5] and numerically in [2], with high accuracy reported.

$$R_{cp} = \frac{1}{\overline{h}A_s} + \frac{1}{2\dot{m}_{cp}c_p} \tag{38}$$

The base conductive thermal resistance, R_{cond} and spreading thermal resistances R_{sp} are both computed using the same models described for the split flow case. The total thermal resistance is then computed from Eqn. 30.

b) Hydraulic Model

The pressure drop in parallel flow is computed from the same models as described for the for the split flow scenario. The only difference is that effective parallel flow length $L_{\rm eff}$ used for split flow modeling is replaced by the total cold plate microchannel, L for parallel flow case, shown in Fig. 3.

II. RESULTS AND DISCUSSION

A. Effect of Jet Slot Aspect Ratio (β) on Performance

Both CFD and analytical thermal resistance predictions agree well, as shown in Fig. 10. Results show that for a fixed flow rate and heat flux, the thermal resistance of split flow cold plate microchannels slightly increases monotonically as the jet slot aspect ratio (β) increases. This is because as β increases, the jet slot widths increases and from mass continuity, the channel velocity decreases, thus reducing the average heat transfer coefficient, which increases the thermal resistance. However, it is key to note that the effect of β on the split flow cold plate thermal resistance is almost insignificant.

Figure 10 also shows good agreement between the CFD model and analytical model pressure drop predictions in split flow configuration cold plate. Results show that the pressure drop significantly decreases with increase in β . This is attributed to reduced channel velocities resulting from mass conservation through the larger jet slots, as β increases. Additionally, from the validated, split flow analytical model [2], [3], it can be reasoned that the total effective flow length, l_{eff} for a split flow microchannel decreases as β increases, thus reducing pressure drop. As such, it is recommended to design split flow cold plates with relatively large β (or jet slot width) to minimize pressure drop without significant penalty on thermal performance.

B. Effect of Channel Aspect Ratio (α) on Performance

From Fig. 11, the CFD model and analytical thermal model results have good agreement, with the maximum error of 8.4% at $\alpha=24$. It is revealed, in Fig. 11, that for fixed flow rate and other thermal conditions, there exists an optimal channel aspect ratio ($\alpha=12$), for which thermal resistance of split flow cold plate minimizes. This is most likely attributed to competing contributing factors for the average heat transfer coefficient, \bar{h} , namely, the channel velocity (or channel Reynolds number) and the heat transfer area. For low channel aspect ratio ($\alpha=6$), the positive contributing effect of higher channel velocity to \bar{h} , is

counteracted by the low heat transfer area of the channels, thus resulting into low \bar{h} and increased thermal resistance. On the other hand, for very high channel aspect ratio $(\alpha=24)$, the contributing positive effect to \bar{h} of higher heat transfer area is counteracted by the associated low channel velocity, which degrades \bar{h} and increases thermal resistance. Notably, for the medium split flow channel aspect ratio $(\alpha=12)$, both positive contributing effects to \bar{h} from heat transfer area and channel velocity probably reach an optimum balance, resulting in relatively higher \bar{h} and thence a relatively lower thermal resistance, in contrast to the other two aforementioned extreme channel aspect ratios.

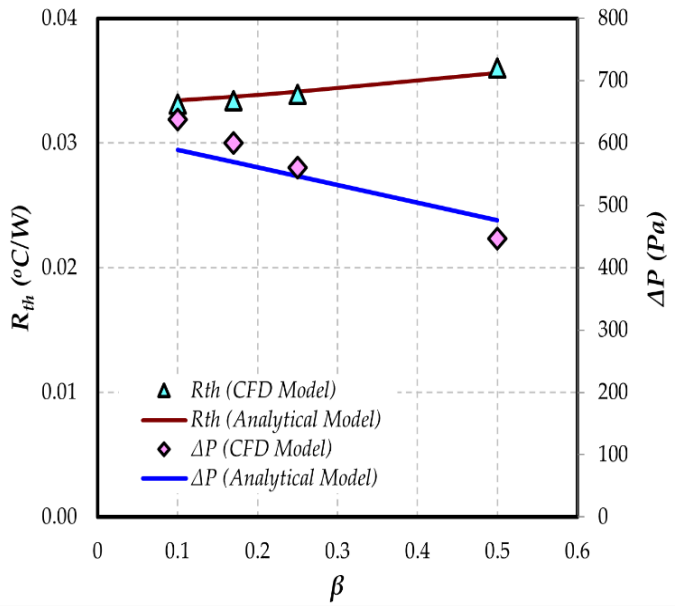


Fig. 10. Effect of jet slot aspect ratio (β) on split flow cold plate microchannel thermal resistance and pressure drop

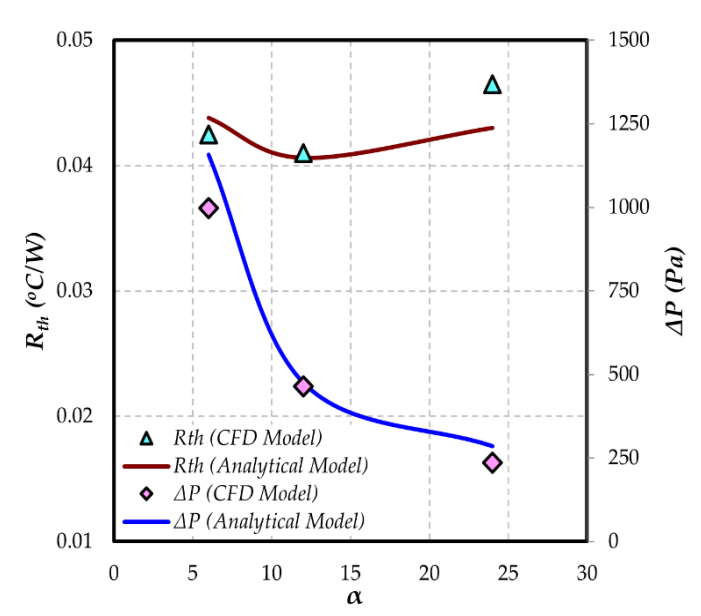


Fig. 11. Effect of channel aspect ratio (α) on split flow cold plate thermal resistance and pressure drop at $\beta = 0.5$ and $\dot{Q} = 0.4$ LPM

At a fixed flow rate, the pressure drop for split-flow cold plates microchannels decreases with increase in channel aspect ratio of split flow cold plates, as shown in Fig. 11. This is because larger channel aspect ratio means larger flow cross-sectional areas, which decrease flow resistance through the microchannels, thus reducing pressure drop. It can be additionally observed that there is no significant reduction in pressure drop by increasing the channel aspect ratio beyond $\alpha = 12$, which was also the optimum α for thermal performance.

C. Effect of Fin Tilt Angle (θ) on Performance

Thermal resistance results from both numerical simulations and thermal analytical model predictions show good agreement for tilted fin channels, as shown in Fig. 12. Channel tilting results from the skiving manufacturing process. Because the flow is vertically downwards at the inlet, flow must turn into the tilted channel as well as outwards, resulting in a more complicated flow turning at the entrance. But results show that split flow thermal resistance is only weakly dependent on fin tilt angle. The same observations were also previously made by Hadad et al. [9]. This is attributed to the two competing effects contributing to heat transfer coefficient. Increasing the split flow fin tilt angle increases the channel Reynolds number, which in turn increase the heat transfer coefficient. However, increasing fin tilt angle decreases the convective heat transfer surface area, which degrades the heat transfer coefficient [2]. As such, it is probable that there is a balance between the two opposing effects on the heat transfer coefficient and the thermal resistance.

On the other hand, the results show that pressure drop strongly depends on fin tilt angle, (θ) , in agreement with observations reported by Hadad et al. [9]. From Fig. 13, the CFD results agree well with the hydraulic analytical model predictions. For a given flow rate, pressure drop monotonically increases with increasing channel tilt (decrease in the fin tilt angle (θ)). The increasingly

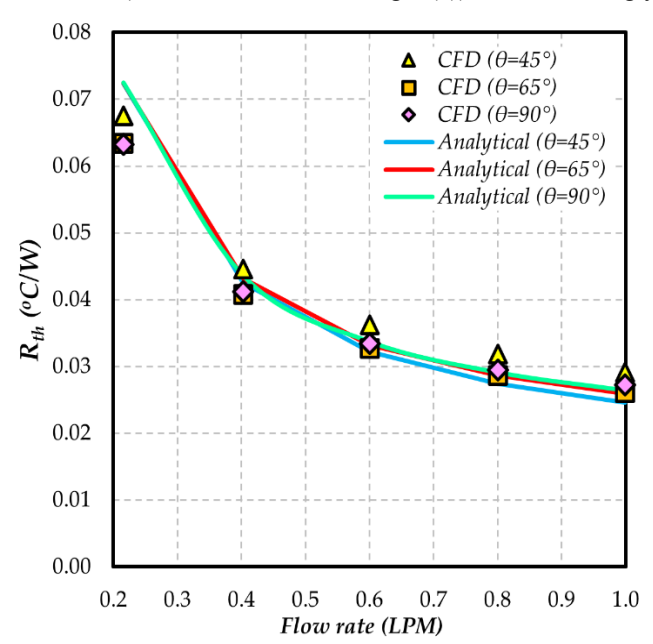


Fig. 12. Effect of fin tilt angle (θ) on split flow microchannel thermal resistance

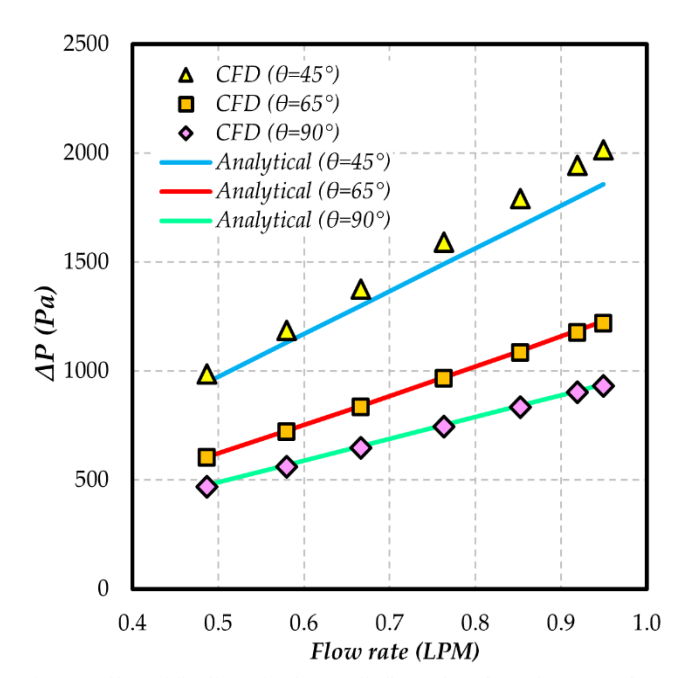


Fig. 13. Effect of fin tilt angle (θ) on split flow microchannel pressure drop

aggressive flow turning into the direction of the channel tilt, followed by the outward flow into the channel causes increased viscous pressure drop [2], [9]. Current results show that vertical finned channels give the least pressure drop and are thus recommended for optimal cold plate design.

D. Performance Comparison of Split flow and Parallel flow Cold Plates

Figure 14 shows that for identical flow, thermal and geometric conditions, the thermal resistances of split flow microchannel cold and the traditional parallel flow microchannels cold plate are extremely similar. Recall that the comparison is made at equivalent total cold plate flow rate, hence the fin channels in the split flow configuration have 50% of the mass flow rate of the parallel flow (side-in side-out) configuration. This is attributed to the phenomenon that flow is divided into two branches, which halves both the flow rate and flow length. Despite the reduction of mass flow rate and hence channel Reynolds number in the split flow configuration, which degrades the heat transfer coefficient, this is largely offset by the shorter flow length leading to higher average heat transfer coefficient due to the thermally developing flow in these shortened channels.

The pressure drop results from numerical simulations and analytical hydraulic model have good agreement, as illustrated in Fig. 15. Results show that, for the same inlet flow rate, split flow cold plate microchannels have up to four times (4X) lower pressure drop compared to the parallel flow cold plate microchannels. Again, this is attributed to the flow branching in the split flow configuration which halves both the flow rate and the flow length, both of which significantly lower the microchannel pressure drop.

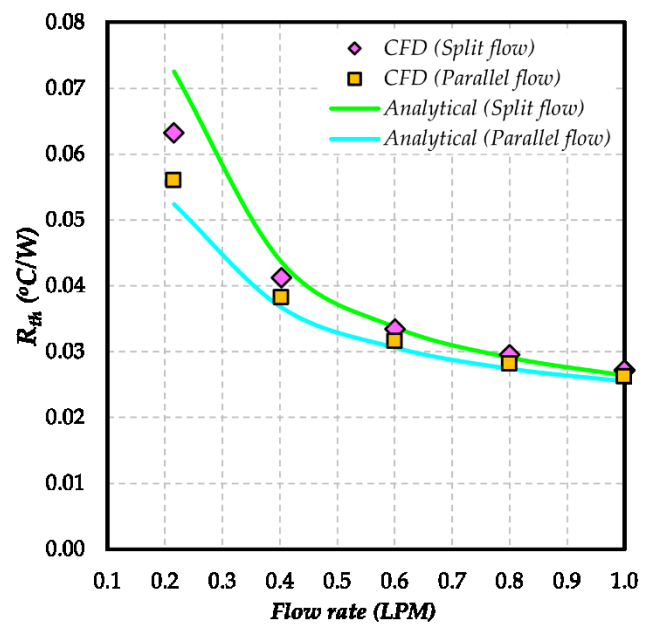


Fig. 14. Comparison of thermal performance (thermal resistance) of split flow and parallel flow microchannel cold plates

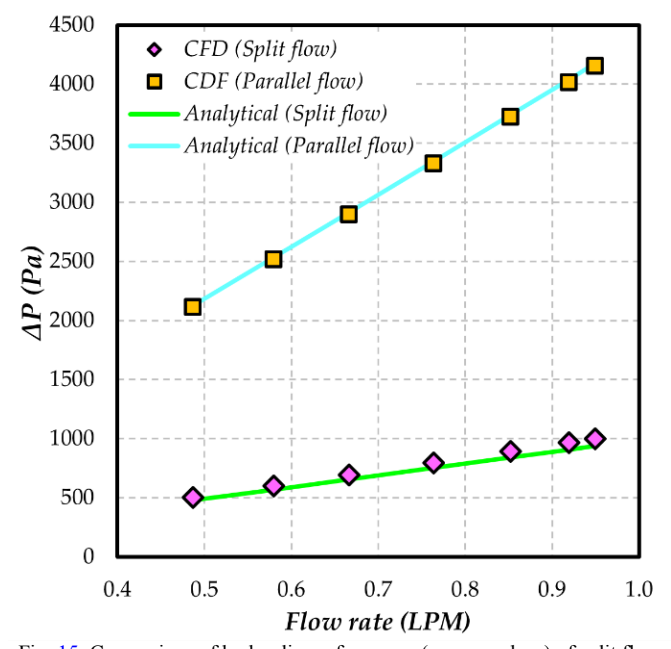


Fig. 15. Comparison of hydraulic performance (pressure drop) of split flow and parallel flow microchannel cold plates

III. CONCLUSIONS

Parametric analyses were performed on the effect of the major geometric aspects, including the jet slot aspect ratios (β) , channel aspect ratios (α) and fin tilt angles (θ) , on the thermohydraulic performance of the split flow microchannel cold plates compared to the conventional parallel flow cold plate.

1. Results show that the thermal resistance of split flow cold plate microchannels is a weak function of jet slot aspect ratio (β) and the pressure drop is strongly dependent on the same. As such, it is recommended to design split flow cold

- plate with relatively higher β 's to minimize pressure drop with no significant effect on the thermal performance.
- 2. There is an optimal channel aspect ratio ($\alpha = 12$) for split flow cold plate at which minimum thermal resistance is attained for this present geometry and conditions. However, pressure drop decreases monotonically with increasing channel aspect (α), though there is almost an insignificant decrease in pressure drop resulting from increasing the channel aspect ratio above $\alpha = 12$.
- 3. Fin tilt angle (θ) has no significant effect on the split flow cold plate thermal resistance, however, increasing it significantly decreases the pressure drop and the minimum is recorded at $\theta = 90^{\circ}$ (vertical finned channels). As such, vertical fins, $\theta = 90^{\circ}$, are recommended for designing an optimized split flow cold plate.
- 4. For the same flow/thermal conditions and dimensions, the thermal performance of split flow and parallel flow microchannel cold plates is almost the same. Most importantly, the pressure drop in split flow microchannels is up to 4 times lower than parallel flow counterparts, for identical conditions, again with little to no penalty on the thermal performance.

ACKNOWLEDGMENT

This work is supported by the National Science Foundation Industry/University Collaborative Research Center (NSF I/UCRC) under Grant No. IIP-1738782. Any opinions, findings, and conclusions or recommendations expressed in this article are solely the responsibility of the authors and do not necessarily represent the official views of the NSF.

REFERENCES

- [1] S. A. Memon, T. A. Cheema, G. M. Kim, and C. W. Park, "Hydrothermal Investigation of a Microchannel Heat Sink Using Secondary Flows in Trapezoidal and Parallel Orientations," *Energies*, vol. 13, no. 21, Art. no. 21, Jan. 2020, doi: 10.3390/en13215616.
- [2] D. Kisitu, "Approximate Compact Thermal-Hydraulic Analytical Models for Laminar Microchannel Impingement Liquid-Cooled Cold Plates for Data Center Thermal Management," M.S.M., Villanova University, United States -- Pennsylvania, 2021. Accessed: Nov. 10, 2022. [Online]. Available:

https://www.proquest.com/docview/2618222739/abstract/20E AA1FC81CD4CC3PQ/1

- [3] D. Kisitu and A. Ortega, "Thermal-Hydraulic Analytical Models of Split-Flow Microchannel Liquid-Cooled Cold Plates With Flow Impingement," presented at the ASME 2021 International Technical Conference and Exhibition on Packaging and Integration of Electronic and Photonic Microsystems, Nov. 2021. doi: 10.1115/IPACK2021-73283.
- [4] H. Modi *et al.*, "Transient CFD Analysis of Dynamic Liquid-Cooling Implementation at Rack Level," presented at the ASME 2022 International Technical Conference and Exhibition on Packaging and Integration of Electronic and Photonic Microsystems, Dec. 2022. doi: 10.1115/IPACK2022-97443.

- [5] H. Y. Zhang, D. Pinjala, T. N. Wong, K. C. Toh, and Y. K. Joshi, "Single-phase liquid cooled microchannel heat sink for electronic packages," *Applied Thermal Engineering*, vol. 25, no. 10, pp. 1472–1487, Jul. 2005, doi: 10.1016/j.applthermaleng.2004.09.014.
- [6] S. G. Kandlikar, "High Flux Heat Removal with Microchannels—A Roadmap of Challenges and Opportunities," *Heat Transfer Engineering*, vol. 26, no. 8, pp. 5–14, Oct. 2005, doi: 10.1080/01457630591003655.
- [7] Y. Hadad, R. Pejman, B. Ramakrishnan, P. R. Chiarot, and B. G. Sammakia, "Geometric Optimization of an Impinging Cold-Plate with a Trapezoidal Groove Used for Warm Water Cooling," in 2018 17th IEEE Intersociety Conference on Thermal and Thermomechanical Phenomena in Electronic Systems (ITherm), May 2018, pp. 673–682. doi: 10.1109/ITHERM.2018.8419540.
- [8] M. K. Sung and I. Mudawar, "Effects of jet pattern on single-phase cooling performance of hybrid microchannel/micro-circular-jet-impingement thermal management scheme," *International Journal of Heat and Mass Transfer*, vol. 51, no. 19–20, pp. 4614–4627, Sep. 2008, doi: 10.1016/j.ijheatmasstransfer.2008.02.021.
- [9] Y. Hadad *et al.*, "Performance Analysis and Shape Optimization of an Impingement Microchannel Cold Plate," *IEEE Transactions on Components, Packaging and Manufacturing Technology*, vol. 10, no. 8, pp. 1304–1319, Aug. 2020, doi: 10.1109/TCPMT.2020.3005824.
- [10] Y. Hadad *et al.*, "Performance analysis and shape optimization of a water-cooled impingement micro-channel heat sink including manifolds," *International Journal of*

- *Thermal Sciences*, vol. 148, p. 106145, Feb. 2020, doi: 10.1016/j.ijthermalsci.2019.106145.
- [11] B. Ramakrishnan, Y. Hadad, S. Alkharabsheh, P. R. Chiarot, and B. Sammakia, "Thermal Analysis of Cold Plate for Direct Liquid Cooling of High Performance Servers," *Journal of Electronic Packaging*, vol. 141, no. 4, Jul. 2019, doi: 10.1115/1.4044130.
- [12] Z. Duan and Y. S. Muzychka, "Impingement air cooled plate fin heat sinks. Part I Pressure drop model," in *The Ninth Intersociety Conference on Thermal and Thermomechanical Phenomena In Electronic Systems (IEEE Cat. No.04CH37543)*, Jun. 2004, vol. 1, pp. 429-435 Vol. 1. doi: 10.1109/ITHERM.2004.1319206.
- [13] D. Copeland, "Optimization of parallel plate heatsinks for forced convection," in *Sixteenth Annual IEEE Semiconductor Thermal Measurement and Management Symposium (Cat. No.00CH37068)*, Mar. 2000, pp. 266–272. doi: 10.1109/STHERM.2000.837093.
- [14] S. Lee, "Calculating Spreading Resistance in Heat Sinks," *Electronics Cooling*, Jan. 09, 1998. https://www.electronics-cooling.com/1998/01/calculating-spreading-resistance-in-heat-sinks/ (accessed Nov. 16, 2022).
- [15] W. M. Kays and A. L. London, "Compact heat exchangers," Jan. 1984, Accessed: Nov. 16, 2022. [Online]. Available: https://www.osti.gov/biblio/6132549